Jurnal Tribologi 35 (2022) 150-166

MYTRIBOS Malaysian Tribology Society

Jurnal Tribologi

Website : jurnaltribologi.mytribos.org e-issn: 2289-7232

Numerical simulation of wheel/rail contact based on DC-FFT and conjugate gradient techniques

Zhijian Wang [1*], Xue Lv [1], Qingtao Yu [2]

[1] School of Mechanical Engineering and Rail Transit, Changzhou University, CHINA.
[2] AVIC Manufacturing Technology Institute, CHINA.
[*]Corresponding author: wangzhijian@cczu.edu.cn

KEYWORD

Wheel/rail contact
DC-FFT
CGM
Cant angle
Yaw angle

ABSTRACT

This paper developed a non-Hertzian contact model, incorporating the contact geometry model and contact mechanics model, to evaluate the contact condition of wheel/rail systems. Discrete convolution-fast Fourier transform (DC-FFT) and conjugate gradient method (CGM) were applied to solve contact model, which can improve the efficiency of the simulation. The model was verified with Kalker's CONTACT program. A systematic parametric analysis was carried out to investigate the influence of lateral displacement, cant angle and yaw angle on wheel/rail contact performance. The results show that large lateral displacement and large yaw angle can significantly deteriorate the contact performance, and the magnitude of lateral displacement influences the choice of cant angle.

Received 24 August 2022; received in revised form 20 September 2022; accepted 13 October 2022.
To cite this article: Wang et al. (2022). Numerical simulation of wheel/rail contact based on DC-FFT and conjugate gradient techniques. Jurnal Tribologi 35, pp.150-166.

NOMENCLATURES

a,b	Grid spacing in two directions
B	Track gauge
d	Distance of two corresponding points on wheel envelope curves and rails
E^*	Modified modulus of elasticity
h	Gap between the two surfaces before deformation
H	Rail height
H'	Vertical displacement
I_c	Set of all grid nodes that are in contact
L	Inside gauge of wheel-set
l_1	Distance from the internal face of the wheel
Q	Normal load
p	Contact pressure
r_0	Wheel radius
u	Surface elastic displacement
V	Measurement point of track gauge
WF	Width of rail foot
x, y, z	Cartesian coordinates

GREEK SYMBOLS

α	Yaw angle
β	Roll angle
γ	Rail cant angle
δ	Approach of two solids

MATRICES

R_{cant}	Transformation matrix
R_1	A function of the yaw and roll angle of the wheelset axle with respect to the track

1.0 INTRODUCTION

Many advances have been made in the field of contact mechanics to predict wheel-rail failure mechanisms, such as the origin of surface cracks, plastic deformation and wear. Generally, the information about wheel/rail contact positions and contact pressure is crucial to predict the wheel/rail performance. Thus, the wheel/rail contact analysis should be further concerned. Two types of stress analysis approaches are often applied in wheel-rail contact problems, i.e. semi-analytical methods and finite element methods (FEM). The principle of semi-analytical method is to use the analytical method to obtain the influence coefficients of pressure-displacement and pressure-stress, then apply numerical techniques, which include variational method (Kalker and Randen, 1972), iterative method (Ahmadi et al, 1983) and conjugate gradient method (CGM) (Polonsky and Keer, 1999), to solve pressure distribution. Kalker and Johnson (990) firstly presented a numerical program CONTACT to deal with wheel/rail contact problems based on minimum principle of the total internal energy. This method can reliably solve general wheel/rail contact. However, it requires too much computational time and therefore cannot realistically be used in online dynamic simulations. To overcome this, some approximate methods have been developed. Kalker (1982) presented the FastSim algorithm based on a simplified theory of rolling contact. Piotrowski and Kik (2008) provided a non-iterative calculation method based on virtual penetration of contacting bodies. Liu et al (2016) further extended the Kik-Piotrowski approach to include the effect of the yaw angle. Although these methods can provide a relatively accurate estimation of the contact patch and contact pressure, they still lack accuracy comparing to the fully numerical solution and FEM (Wiest et al., 2006; Wen et al., 2011; Ma et al., 2018). The FEM is generally accurate but is also time-consuming. Thus, the advancements of numerical techniques were necessary to improve the computational efficiency of wheel/rail contact problems.

The fast calculation of surface deflection and the rapid convergence of numerical methods are two key points in contact problems. In recent decades, by applying Fast Fourier transform (FFT) (Liu et al., 2000) or the multigrid multi-integration techniques (Brandt and Lubrecht, 1990), the computational time of surface deflection is reduced by orders of magnitude, as compared to conventional algorithms. In addition, the use of CGM largely reduces the number of iterations required for solving problems with huge number of grids. Hence, these new numerical techniques are now fast enough to solve contact problems. Unfortunately, these new methods are rarely applied in wheel/rail contact analysis. Vollebregt (2014) and Barbinta et al (2014) were the first to take advantages of new approaches in modelling wheel/rail contact. The effects of lateral displacement and rail inclination under different wheel/rail profile conditions on the contact patch and contact pressure were discussed. The few shortcomings of their model are that the separation between contacting surfaces did not take the influences of roll angle and yaw angle into account, and the contact geometrical relationship of real wheel/rail system was not established to determine the contact points before conducting contact simulation.

In this work, a coupled model was developed, incorporating the contact geometry model and contact mechanics model, to evaluate the contact performance of wheel/rail systems. For the contact geometry program, a new numerical iteration method was presented to determine the initial contact points of the wheel/rail system. For the contact mechanics program, DC-FFT and CGM were applied to conduct contact simulation. Finally, the model developed by this work is applied to investigate effects of lateral displacement, cant angle and yaw angle on the wheel/rail contact performance.

2.0 MODEL

2.1 Determination of Contact Points

Figures 1 and 2 give the coordinate systems of track and wheelset. *O-xyz* defined as an inertial frame; the *x* axis is parallel to the track in the point *O* and z axis is normal to the ground. O_{r1}-x_{r1} y_{r1} z_{r1} and O_{r2}-x_{r2} y_{r2} z_{r2} are the body fixed frames of left rail and right rail respectively; O_{r1_1}-x_{r1_1} y_{r1_1} z_{r1_1} is the auxiliary frame; γ is the rail cant angle. *B* is the track gauge; *V* is the measurement point of track gauge; *WF* is the width of rail foot. O_c-x_c y_c z_c is the body fixed frame of the wheelset, where its origin O_c is fixed in the center of the wheelset. y_w is the lateral displacement; α is the yaw angle; β is the roll angle; r_0 is the wheel radius; *H* is the rail height; *H'* is the vertical displacement; *L* is the inside gauge of wheel-set; l_1 is the distance from the internal face of the wheel; O_{w1}-x_{w1} y_{w1} z_{w1} and O_{w2}-x_{w2} y_{w2} z_{w2} are the body fixed frames of left wheel and right wheel respectively.

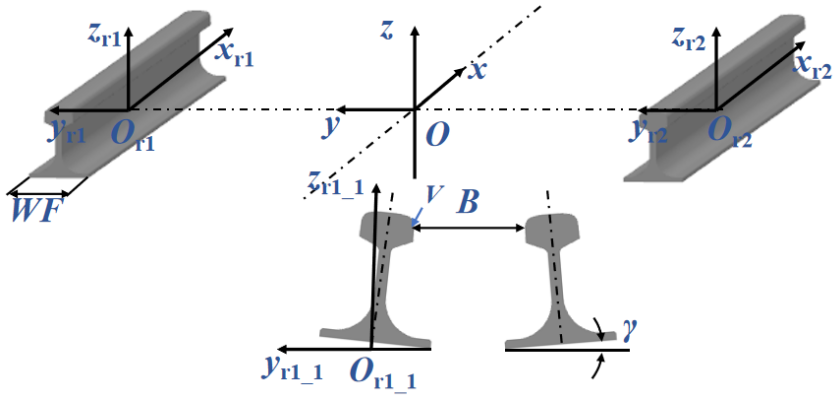

Figure 1: Coordinate system of track.

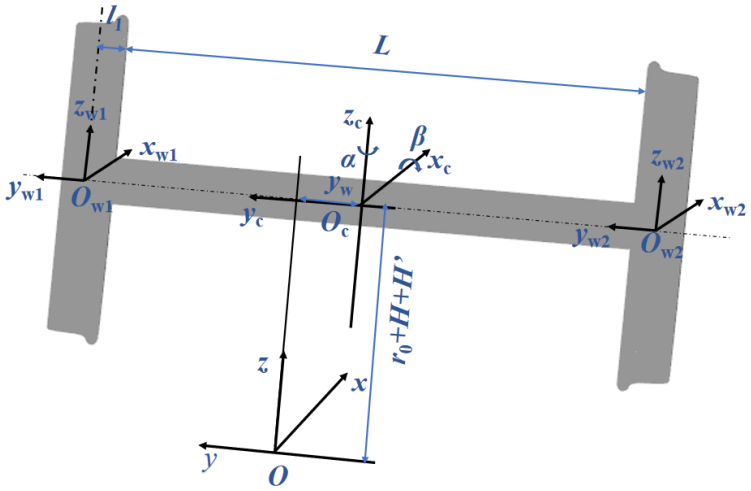

Figure 2: Coordinate system of wheel-set.

In order to obtain the initial contact points of the wheel/rail system, introducing the distance functions $d_1(x_{w1}, y_{w1})$ and $d_2(x_{w2}, y_{w2})$, which measure the distance of two corresponding points on wheel envelope curves and rails in the z_{w1}/z_{w2}-direction, as shown in Figure 3. These two functions need to satisfy the following constraints simultaneously:

$$\min(d_1) = \min(d_2) = 0 \tag{1}$$

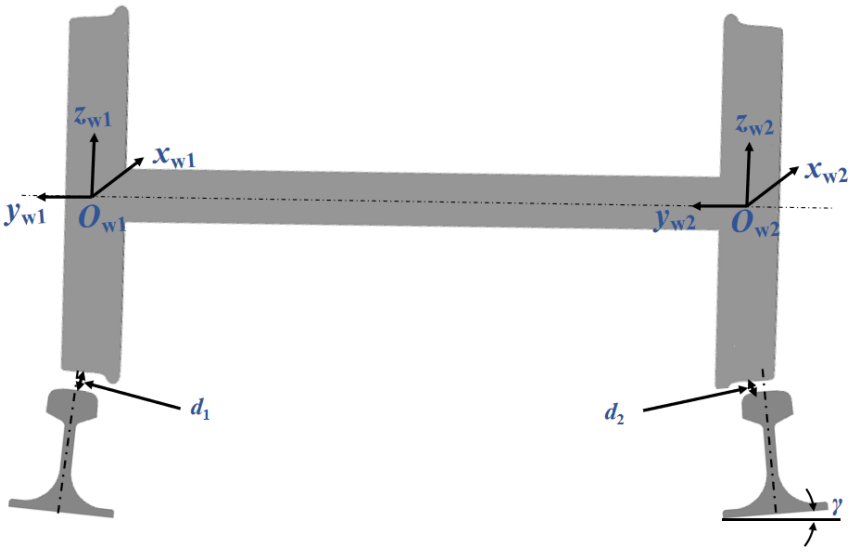

Figure 3: The schematic of distance function.

The distance functions can be expressed by the coordinate transformation method. Take d_1 for example:

(a) Any point on the rail surface is expressed in the body fixed frame of left rail as follows, which depends on the rail profile.

$$S_{r1} = f(x_{r1}, y_{r1}, z_{r1}) \tag{2}$$

(b) S_{r1} is transformed from the body fixed frame of rail to the body fixed frame of wheel according to the following operations

First , S_{r1} is transformed from the body fixed frame of rail to O_*xyz* coordinate system by

$$S_{r1\_o} = [R_{cant}]\left[\begin{pmatrix} x_{r1} \\ y_{r1} \\ z_{r1} \end{pmatrix} + \begin{pmatrix} 0 \\ WF/2 \\ 0 \end{pmatrix}\right] + \begin{bmatrix} 0 \\ B/2 - V_y \\ 0 \end{bmatrix} \tag{3}$$

where S_{r1_o} is the coordinates of any point on the rail surface in the O_*xyz* coordinate system. V_y is the y coordinate of point V in the auxiliary frame O_{r1_1}-x_{r1_1} y_{r1_1} z_{r1_1}. $[R_{cant}]$ is the transformation matrix and is defined as:

$$[R_{cant}]=\begin{pmatrix}\cos\gamma & -\sin\gamma & 0\\ \sin\gamma & \cos\gamma & 0\\ 0 & 0 & 1\end{pmatrix} \tag{4}$$

Second, S_{r1_o} is transformed from O_*xyz* coordinate system to the body fixed frame of wheel O_{w1}-x_{w1} y_{w1} z_{w1}.

$$S_{r1\_w}=[R_1]\left[\begin{pmatrix}S_{r1\_o}(1)\\ S_{r1\_o}(2)\\ S_{r1\_o}(3)\end{pmatrix}+\begin{pmatrix}0\\ 0\\ r_0+H+H'\end{pmatrix}\right]-\begin{bmatrix}0\\ L/2+y_w+l_1/2\\ 0\end{bmatrix} \tag{5}$$

where, S_{r1_w} is the coordinates of any point on the rail surface in the O_{w1}-x_{w1} y_{w1} z_{w1} coordinate system. The matrix $[R_1]$ is defined as a function of the yaw and roll angle of the wheelset axle with respect to the track:

$$[R_1]=\begin{pmatrix}\cos\alpha & -\sin\alpha\cos\beta & \sin\alpha\sin\beta\\ \sin\alpha & \cos\alpha\cos\beta & -\cos\alpha\sin\beta\\ 0 & \sin\beta & \cos\beta\end{pmatrix} \tag{6}$$

(c) According to the position of rail surface in the body fixed frame of wheel, the corresponding point on the wheel surface, $S_{w1,}$ can be calculated

$$S_{w1}=\begin{bmatrix}S_{r1\_w}(1)\\ S_{r1\_w}(2)\\ z_{w1}\end{bmatrix} \tag{7}$$

(d) Finally, the expression of distance function d_1 can be written as:

$$d_1=S_{w1}(3)-S_{r1\_w}(3) \tag{8}$$

Similarly, the expression of distance function d_2 can be calculated. The magnitude of distance functions depends on the wheel/rail profile, lateral displacement, vertical displacement, yaw angle and roll angle, where vertical displacement and roll angle are the two unknown parameters. During the numerical calculation, these two parameters can be adjusted to meet the requirements of Equation (1). The detailed calculation procedure is shown in Figure 4.

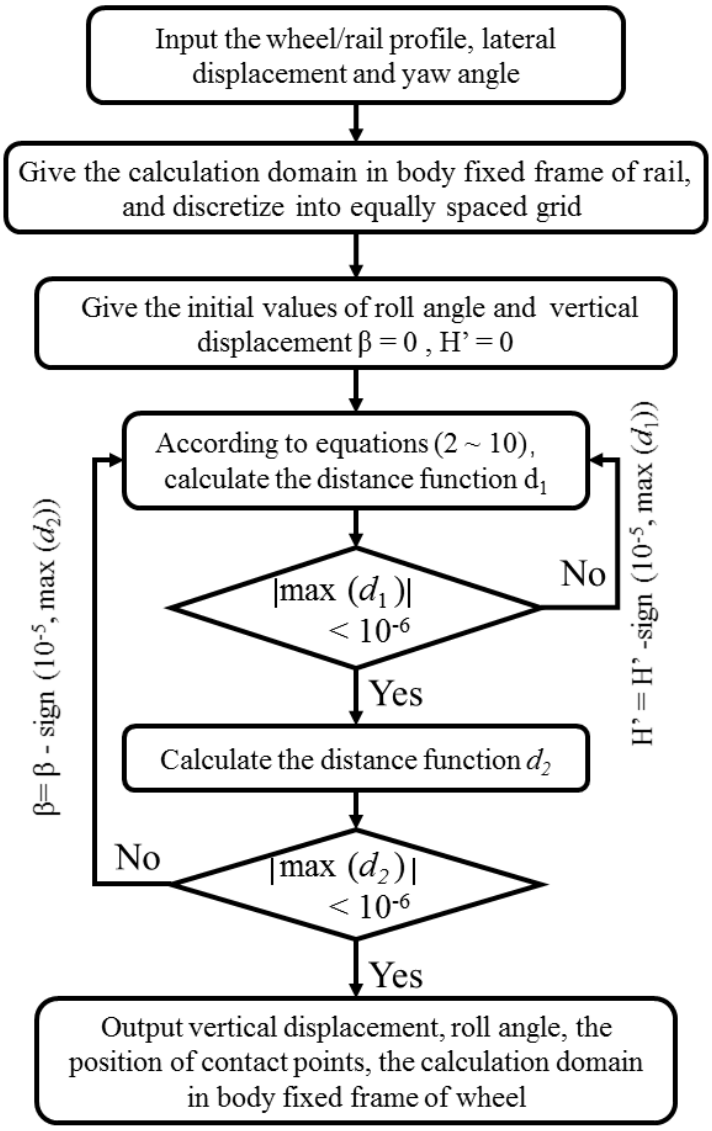

Figure 4: Flowchart of contact points determination.

2.2 Contact Model

The wheel-rail contact problem is often beyond the scope of Hertz theory due to the complex profile of wheel/rail. It is a non-Hertzian contact problem. In this work, the wheel-rail contact is assumed to work under elastic deformation. The elastic non-Hertzian contact problem can be described by the basic Equations and inequalities describing the relations of contact geometry, pressure and deformation (Johnson, 1985):

$$u_{ij} = -h_{ij} + \delta, \quad (i,j) \in I_c \tag{9.1}$$

$$p_{ij} > 0, \quad (i,j) \in I_c \tag{9.2}$$

$$u_{ij} \geq -h_{ij} + \delta, \quad (i,j) \notin I_c \tag{9.3}$$

$$p_{ij} = 0, \quad (i,j) \notin I_c \tag{9.4}$$

$$a \times b \times \sum_{(i,j) \in I_c} P_{ij} = Q \tag{9.5}$$

$$u_{ij} = \frac{1}{\pi E^*} \iint \frac{P_{kl}}{\sqrt{(x_k - x_i) + (y_l - y_j)}} dkdl \tag{9.6}$$

Here, u is the surface elastic displacement; h is the gap between the two surfaces before deformation and it can be described as the distance functions; δ is the approach of two solids; a and b are the grid spacing in two directions; and I_c is the set of all grid nodes that are in contact. The surface elastic deformation function, described in (9.6), presents a linear convolution expression that is solved using DC-FFT algorithm. Liu et al. [11] presented different methods to solve the linear convolution expression. It was found that found that the DC-FFT algorithm is the most efficient approach for linear convolution expression. It should be noted that the discretization of calculation domain must be equally spaced when using the DC-FFT algorithm, while the obtained calculation domain under the body fixed frame of wheel was not equally spaced discretized due to the coordinate transformation. Thus, the calculation domain under the body fixed frame of wheel needs to be remeshed at equally spaced grid and the distance functions need also to be recalculated. The solution of distance function requires the following steps:

(a) Discretize calculation domain under the body fixed frame of the wheel into equally spaced grid.
(b) Calculate the z-coordinates of the wheel envelope curve in the body fixed frame of the wheel for every mesh grid.
(c) Transform points on the wheel envelope curve from the body fixed frame of the wheel to the body fixed frame of the rail.
(d) Use the x and y coordinates of this transforming point in the body fixed frame of the rail to calculate the z coordinate of rail surface in the body fixed frame of the rail.
(e) Compare the value of z-coordinate between rail surface and transforming point in the body fixed frame of the rail, if the value is equal, go to the next step; or change the value of z-coordinate of the transforming point in the body fixed frame of the wheel and go to step c, until two values are equal.
(f) Calculate the distance between the wheel envelope curve and rail surface under the body fixed frame of the wheel at mesh grid, which is equal to z-coordinates of wheel envelope curve minus z-coordinate of updated transforming point in the body fixed frame of the wheel.

Once the distance is obtained, which can replace the h in Equation 9.1. Equations 9.1~9.6 are solved for the contact patch and contact pressure which gives important information about contact performance. The set of contact nodes I_c, a discrete analogue of the real area of contact, is not generally known in advance and needs to be calculated as part of problem solution. Usually, the normal load Q is specified, while the approach δ is unknown. In the present work, the adopted technique for the solution scheme is based on the conjugated gradient technique usually used for unconstrained optimization. Then they were extended to solve quadratic optimization problems

with linear inequality constraints, such as the contact problem. For more details about the iteration scheme, the reader may refer to reference [3].

2.3 Validation

In order to validate the proposed contact model, the results from Kalker's CONTACT program was used to compare with that from the present model. The calculation parameters applied for simulation are listed in Table 1.

Figure 5 and Table 2 give a set of comparisons among two different models. It can be found that the lateral displacement has a strong influence on the contact patch, and the present results are in correlation with Kalker's results. The error of the maximum contact pressure between two different programs is less than 6%, and the shape of the contacts is basically the same, which validates the proposed contact model in this work. These tests are run with a Fortran program on a commodity Windows laptop. It has an Intel Core i5 – 3230 cpu at 2.60 GHz and 12.0 GB physical memory. The program includes three modules: contact geometry module, remesh module, contact mechanics module. The total cpu time for solving a case with 256 × 128 elements is about 8.25 seconds. The computational efficiency of the present model may be improved by parallel algorithm and contact position prediction.

Table 1: Calculation parameters.

Parameter type	**Value**
Wheel/rail profile combination	S1002/UIC60
Track gauge	1435 mm
Rail cant angle	1:40
Inner gauge of the wheelset	1360 mm
Wheel radius	460 mm
Distance from wheel tread to its internal face	70 mm
Young's modulus	210 GPa
Poisson's ratio	0.3

Table 2: Error of the maximum contact pressure.

Lateral displacement (mm)	-5	-3	-1	1	3	5
Results from [7] (MPa)	1093	1030	829	1220	1495	2278
The present model (MPa)	1115	1010	852	1165	1470	2150
Error	2.2%	1.9%	2.7%	4.5%	1.7%	5.6%

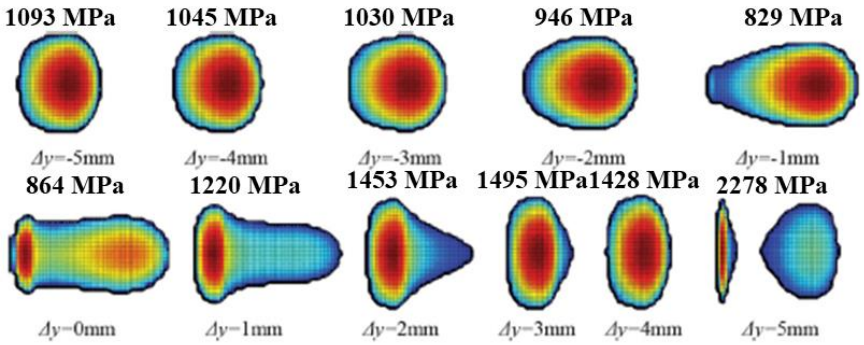

(a) Results of CONTACT program (Liu et al., 2016).

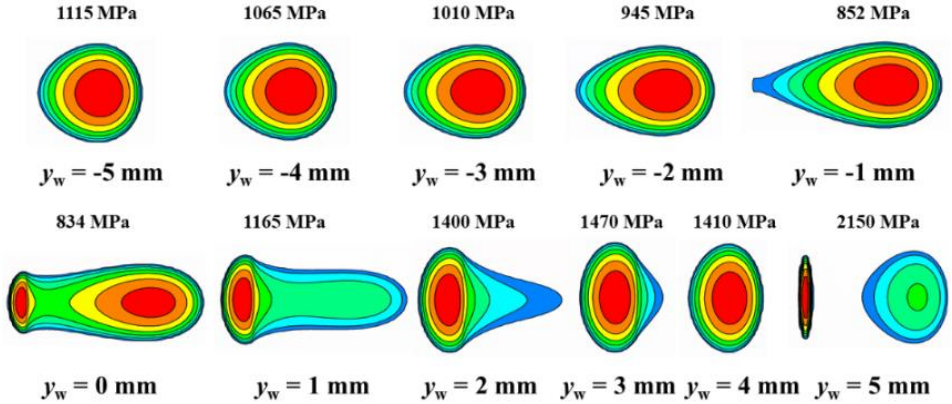

(b) Results of the proposed contact model

Figure 5: Contact patch variation with the lateral displacement.

3.0 RESULTS AND DISCUSSION

In this section, the simulations were performed on a LM-type worn tread profile and 60 kg/m rail inclined at 1/40. Here the wheel has a radius of 420 mm in the rolling direction, the inner gauge of the wheelset is 1360 mm, and the track gauge is 1435 mm. Mathematical Equations of wheel/rail profiles are established based on China's National Standard for Passenger Train Wheels and Rails (TB/T 449, 2003; GB 2585, 2021).

3.1 Effects of Lateral Displacement

The test of wheelset displacement has shown that lateral displacements of all wheelsets are less than 10 mm Wang et al., 2022). Here, the lateral displacement varies from -10 mm to 10 mm in 1 mm increment. Figure 6 shows the variation of contact positions with lateral displacement of wheelset. For the left wheel/rail contact, it can be found that the contact point moves from 20.0 mm to -37.0 mm in the body fixed frame of the wheel, and from 1.5 mm to -32.5 mm in the body fixed frame of the rail. That is to say the contact position moves from wheel tread to wheel flange, and from rail head to rail gauge, while wheel and rail rarely come into contact in field side. In addition, the range of the contact position is smaller with small lateral displacement. For the right

wheel/rail contact, it can be found that the contact point moves from 37.0 mm to -20.0 mm in the body fixed frame of the wheel, and from 32.5 mm to -1.5 mm in the body fixed frame of the rail. That is to say the contact position moves from wheel flange to wheel tread, from rail gauge to rail head, and wheel and rail also rarely come into contact in field side. It is also found that when the lateral displacement from 8 to 10 and from -8 to -10, the slope of the curve suddenly changes. This is due to the variation of curvature of the wheelset and rail curves.

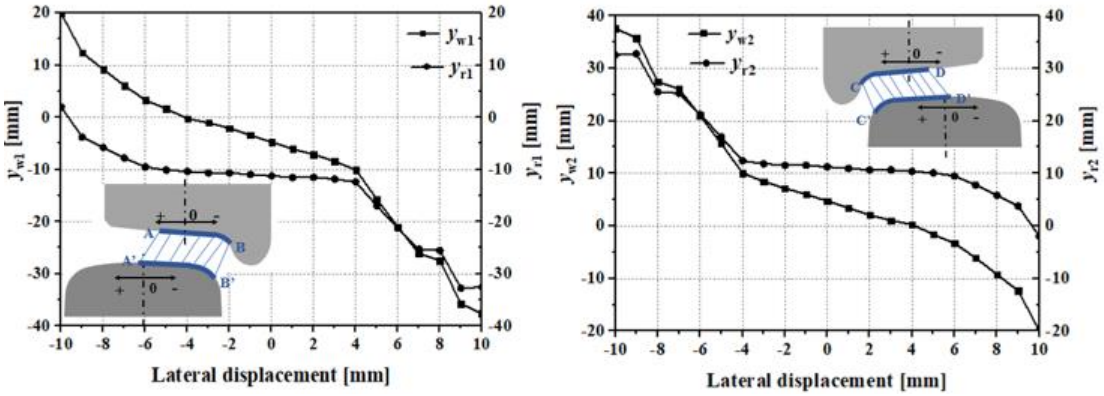

(a) Left wheel/ rail contact (b) Right wheel/rail contact

Figure 6: Variation of positions of contact points with lateral displacement.

Figure 7 shows the variation of roll angle with lateral displacement. It can be found that when the lateral displacement is negative, the roll angle is positive, and the roller angle increases with increasing the magnitude of lateral displacement. In addition, when the lateral displacement is positive, the roll angle is negative, and the roller angle also increases with increasing the magnitude of lateral displacement.

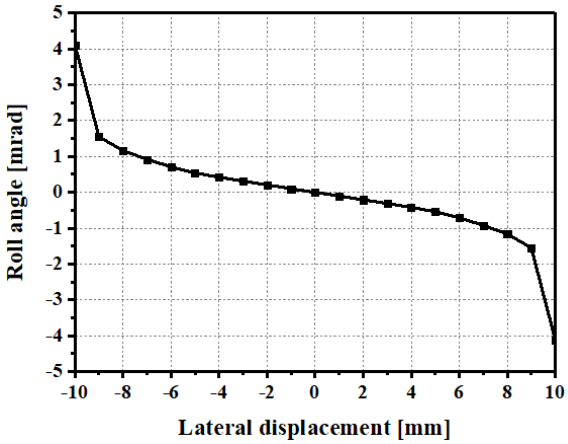

Figure 7: Variation of roll angle with lateral displacement.

Figure 8 shows the variations of contact patch and the maximum contact pressure with lateral displacements. It can be noticed that the lateral displacement of the wheelset has a strong

influence on both the shape of the real contact area and the maximum contact pressure. For the left wheel/rail contact, the trend of variation of the maximum contact pressure with increasing lateral displacements can be divided into three parts: a mild increase when the lateral displacement is less than 0 mm, followed by a sharp decrease, and a sharp increase. The sharp increase is due to the wheel flange-rail gauge contact. For the right wheel/rail contact, the variation tendency is opposite. Thus, results from Figure 6 to Figure 8 suggest that the lateral displacement should be below a certain magnitude to avoid wheel flange-rail gauge contact.

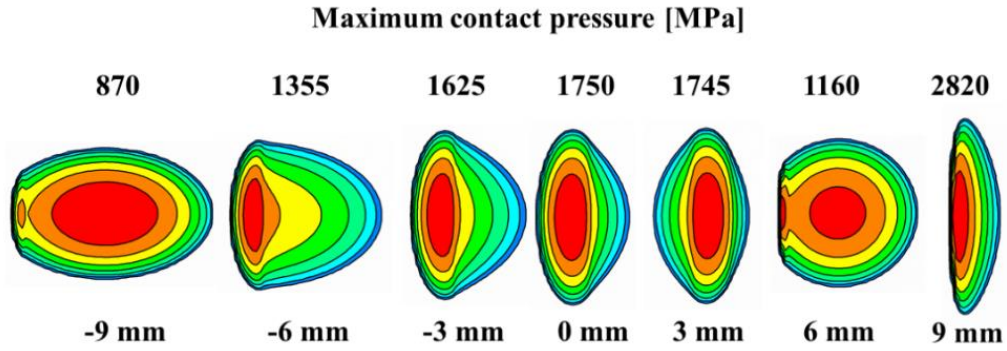

(a) Left wheel/rail contact

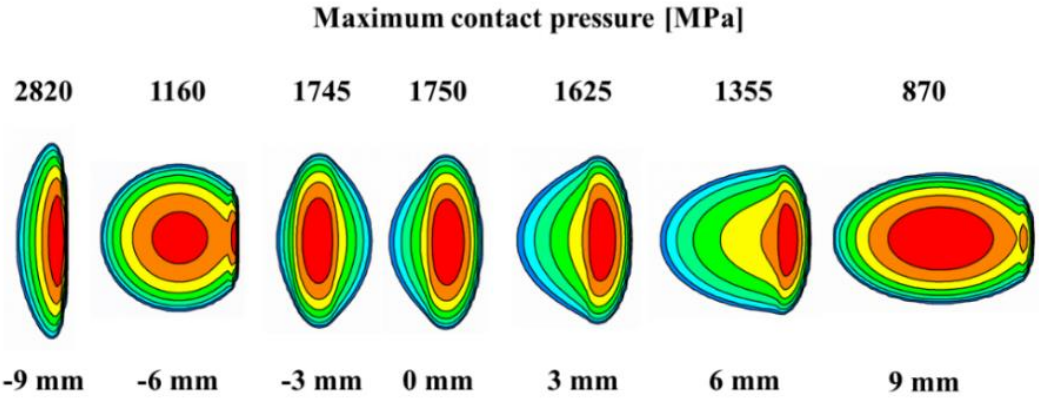

(b) Right wheel/rail contact

Figure 8: Contact patch and maximum contact pressure under different lateral displacements.

3.2 Effects of Rail Cant

The standard value of rail cant differs throughout the international railway community, and the most common values of rail cant are 1:20, 1:30 and 1:40 (Jabbar-Ali, 2011). Here, the value of 1:20 and 1:30 is chosen to discuss. Figure 9 shows the variation of roll angle with lateral displacement under different cant angle. It can be found that as the lateral displacement increases, the magnitude of roll angle increases. In addition, as the cant angle increases, the magnitude of roll angle decreases. Figure 10 gives the variation of positions of contact point with lateral displacement under different cant angle for the left wheel/rail contact, it can be found that the variation range of the position of contact points is wider for large rail cant angle. In the current

working conditions, when the lateral displacement ranges from -8mm to 8mm, the variation range of the position of contact points for the rail cant of 1:20 is 45mm, while the variation range for the rail cant of 1:30 is 40mm. In addition, the slop of variation decreases with decreasing cant angle. When the lateral displacement varies from -2mm to 4mm for the cant angle of 1:30, the location of contact points in rail is almost unchanged due to the influences of profiles of wheelsets and rails. Cui et al (2019) obtained the similar results. Thus, results in Figure 9 and Figure 10 indicate that the rail cant angle has a major influence on roll angle and positions of contact points

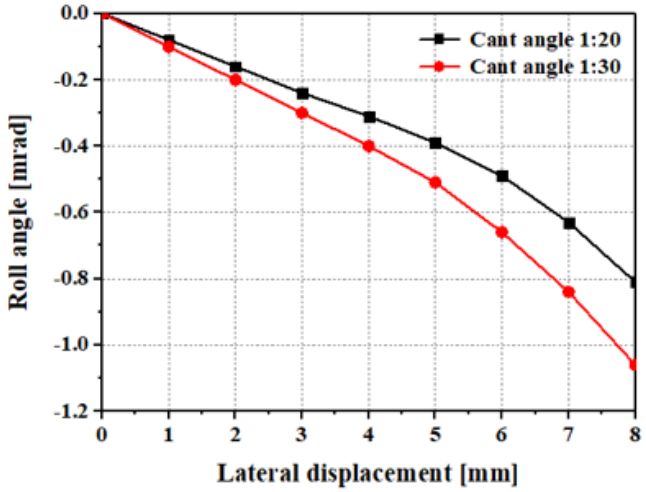

Figure 9: Variation of roll angle with lateral displacement under different cant angle.

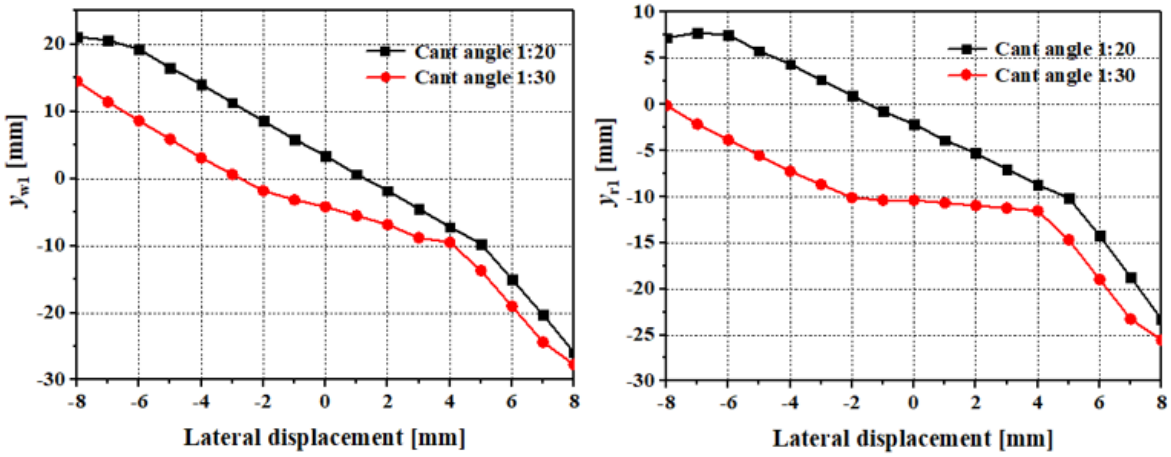

Figure 10: Variation of positions of contact point with lateral displacement under different cant angle for left wheel/rail contact.

Figure 11 compares the contact patch and the maximum contact pressure under two different cant angles for left wheel/rail contact, the first row is the results of cant angle 1:20, the second row is the results of cant angle 1:30. From the figure, it can be found that when the lateral

displacement is less than 3 mm, the maximum contact pressure under cant angle 1:20 is lower than that under cant angle 1:30, while the lateral displacement is larger than 3 mm, the maximum contact pressure under cant angle 1:20 is higher than that under cant angle 1:30. The results in Figure 10 implies that when the wheelset passes a straight track, the rail with cant angle 1:20 is superior to cant angle 1:30 in terms of contact pressure; while the wheelset passes a curve track, the rail with cant angle 1:30 is superior to cant angle 1:20 in terms of contact pressure.

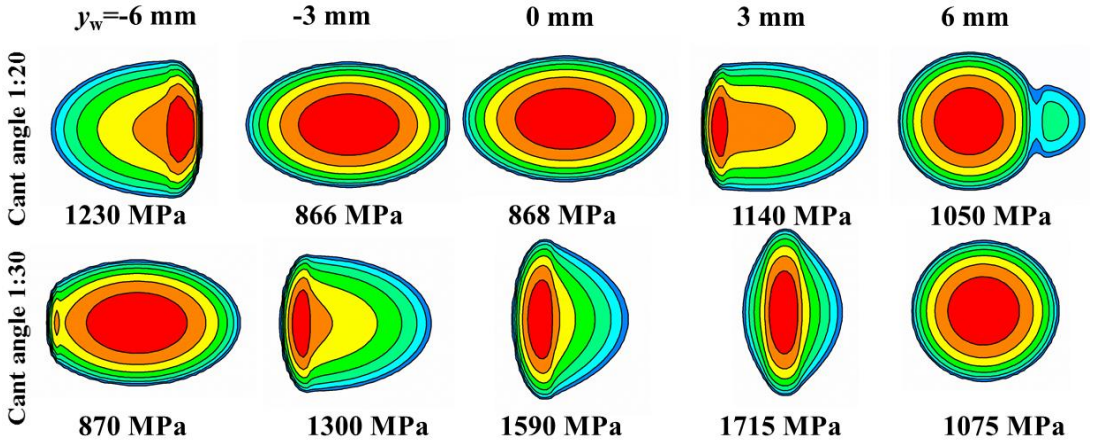

Figure 11: Variation of positions of contact patch and the maximum contact pressure with lateral displacement under different cant angle for left wheel/rail contact.

3.3 Effects of Yaw Angle

Figure 12 shows the variation of roll angle with yaw angle under different lateral displacements, it can be found that when the yaw angle varies from 0 mrad to -0.05 mrad, the magnitude of the roll angle increases for all cases in the current analysis; while the yaw angle varies from 0 mrad to 0.05 mrad, the magnitude of the roll angle increases when the lateral displacement is 0 mm, and decreases when the lateral displacement is greater than 0 mm. In addition, its slope increases with increasing lateral displacement, especially for large negative yaw angle. The results in this figure imply that the effect of yaw angle on roll angle is significant when the raw angle is large, especially accompanied with a large lateral displacement.

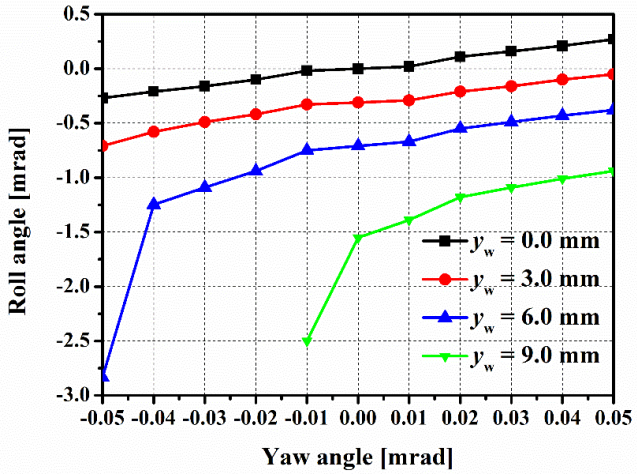

Figure 12: Variation of roll angle with yaw angle under different lateral displacement.

Figure 13 shows the variation of the contact patch and the maximum contact pressure with different yaw angle when the lateral displacement is equal to 6 mm, the first row is the results of left wheel/rail contact, and the second row is the results of right wheel/rail contact. From the figure, it can be found that as the yaw angle varies, the shape of the contact patch and the maximum contact varies. In addition, when the wheelset produces any yaw movement, the maximum contact pressure of the wheel/rail contact increases regardless of the direction of yaw angle, and when the yaw angle is negative, the maximum contact pressure of the left wheel/rail contact sharply increases; while the yaw angle is positive, the maximum contact pressure of right wheel/rail contact mildly increases. Thus, in current cases the mild yaw angle, combined with mild lateral displacement, will significantly deteriorate contact performance.

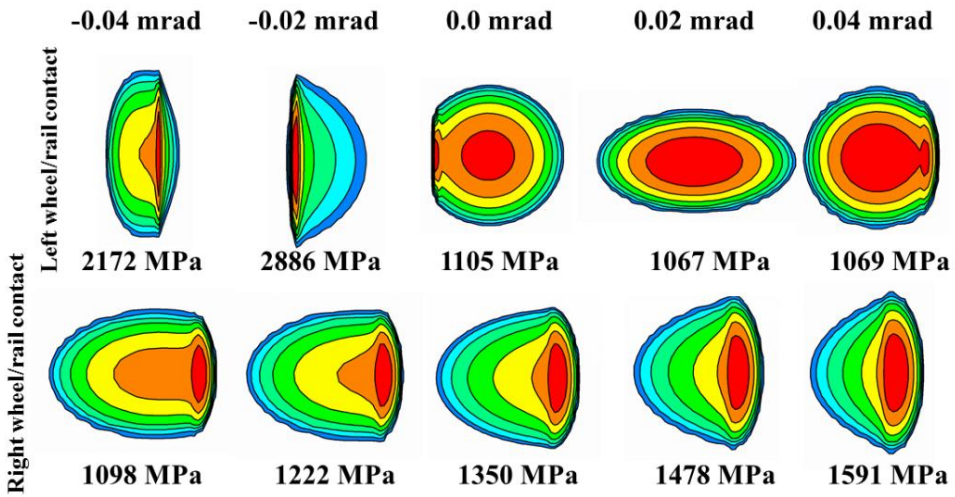

Figure 13: Variation of contact patch and maximum contact pressure with yaw angle under lateral displacement y_w = 6 mm.

CONCLUSIONS

In this study, a non-Hertzian contact model evaluating wheel/rail contact performance was established. This model incorporates a contact geometry program and a contact mechanics program. In order to improve the simulation efficiency, the advanced numerical calculating method, including DC-FFT and CGM, were applied. The results of the presented model were compared to the results from Kalker's CONTACT, to demonstrate credibility of the proposed model. Then, parametric analyses were conducted to investigate the influence of lateral displacement, cant angle and yaw angle on contact performance. Some conclusions drawn from this study are shown as follows:

(a) As the lateral displacement varies from -9 mm to 9 mm, the position of contact point for left wheel/rail contact would move from wheel tread to wheel flange, and from rail head to rail gauge. And when the wheel flange contacts the rail gauge, the wheel/rail contact condition sharply deteriorate.

(b) When the lateral displacement of the wheelset is less than 3 mm, the rail with cant angle 1:20 is superior to that with a cant angle 1:30 in terms of contact condition; while cant angle 1:30 is superior when the lateral displacement of the wheelset is greater than 3 mm.

(c) As the yaw angle varies, the shape of the contact patch and the maximum contact changes sharply. Mild yaw angle, combined with mild lateral displacement, will significantly deteriorate contact condition.

ACKNOWLEDGEMENTS

This work is financially supported by Natural science fund for colleges and universities in Jiangsu Province (No.20KJD460002) and Scientific Research Foundation of Changzhou University.

REFERENCES

Ahmadi, N., Keer, L. M., Mura, T., 1983. Non-Hertzian contact stress analysis for an elastic half space—normal and sliding contact. International Journal of Solids & Structures, 19(4):357-373.

Barbinta, C. I., Ulianov, C., Franklin, F., 2014. Wheel-rail contact modelling and analysis, considering profiles types and lateral displacement. Transport Research Arena: 5th Conference: Transport Solutions from Research to Deployment, Paris, France.

Brandt, A., Lubrecht, A. A., 1990. Multilevel matrix multiplication and fast solution of integral Equations. Journal of Computational Physics, 90(2):348-370.

Cui, D., Wang, R., Allen, P., 2019. Multi-objective optimization of electric multiple unit wheel profile from wheel flange wear viewpoint. Struct Multidisc Optim, 59, 279–289.

GB 2585, 2021, Hot-rolled steel rails for railway.

Jabbar-Ali Zakeri, Masoud Fathali, Nima Boloukian R., 2011. Effects of Rail Cant on Wheel-Rail Contact Forces in Slab Tracks. International Journal of Mechanics and Applications, 1(1), pp. 12-21.

Johnson, K. L., 1985. Contact Mechanics. Cambridge: Cambridge University Press.

Kalker, J. J and Randen, Y. V., 1972. A minimum principle for frictionless elastic contact with application to non-Hertzian half-space contact problems. Journal of Engineering Mathematics, 6(2):193-206.

Kalker, J. J. and Johnson, K. L., 1990. Three-Dimensional Elastic Bodies in Rolling Contact, Kluwer Academic pub.

Kalker, J. J., 1982. A Fast Algorithm for the Simplified Theory of Rolling Contact. Vehicle System Dynamics, 11(1):1-13.

Liu, B., Bruni, S., Vollebregt, E., 2016. A non-Hertzian method for solving wheel-rail normal contact problem taking into account the effect of yaw. Vehicle System Dynamics, 54(9):1226-1246.

Liu, S., Wang, Q., Liu, G., 2000. A versatile method of discrete convolution and FFT (DC-FFT) for contact analyses. Wear, 243(1–2):101-111.

Ma, Y., Markine, V. L., Mashal, A. A., 2018. Improving the performance of finite element simulations on the wheel–rail interaction by using a coupling strategy. Proceedings of the Institution of Mechanical Engineers Part F Journal of Rail & Rapid Transit, 2018:095440971774598.

Piotrowski, J and Kik, W., 2008. A simplified model of wheel/rail contact mechanics for non-Hertzian problems and its application in rail vehicle dynamic simulations. Vehicle System Dynamics, 46(1-2):27-48.

Polonsky, I. A., Keer, L. M., 1999. A numerical method for solving rough contact problems based on the multi-level multi-summation and conjugate gradient techniques. Wear, 231(2):206-219.

TB/T 449, 2003, Wheel profile for locomotive and car.

Vollebregt, E. A. H., 2014. A new solver for the elastic normal contact problem using conjugate gradients, deflation, and an FFT-based preconditioner. Journal of Computational Physics, 257:333-351.

Wang, Ping, Chen, Rong , Quan, 2022. Development and Application of Wheel-set Lateral Displacement Test System in High Speed Railway Turnout Zone. Przeglad Elektrotechniczny, 88. 69-73.

Wen, Z., Wu, L., Li, W., 2011. Three-dimensional elastic–plastic stress analysis of wheel–rail rolling contact. Wear, 271(1):426-436.

Wiest, M., Kassa, E., Daves, W., 2006. Assessment of methods for calculating contact pressure in wheel-rail/switch contact. Wear, 265(9):1439-1445.